DESIGN AND EXPERIMENT OF RIDGE HEIGHT ADAPTIVE ADJUSTMENT SYSTEM FOR CRAWLER-TYPE RIDGER
/
履带式起垄机垄高自适应调节系统设计与试验

Qikai DONG*), **Xiaoying WANG**, **Weijian ZHENG**, **Yifan YAO**, **Tianyu YANG**
College of Agricultural Engineering and Food Science, Shandong University of Technology, Zibo 255000, China;
Corresponding author: Dong Qikai
Tel: +86-19811718151; E-mail: 1436176342@qq.com

DOI: https://doi.org/10.35633/inmateh-77-111

Keywords: *ridger; ridge height; PID control; adaptive adjustment*

ABSTRACT
Aiming at the problem of poor adaptability and insufficient stability of ridge height caused by hilly terrain, this study designed an adaptive ridge height adjustment system for crawler ridger. By analyzing the process of ridging operation, the mathematical model of ridge height control is established, and the control strategy based on incremental PID is used to dynamically adjust the push rod expansion of hydraulic cylinder in real time, so as to realize the precise adjustment of machine lifting. Combined with the inertial measurement unit, the pitch angle and height information of the vehicle body are collected in real time, and the ridge height is dynamically compensated. The field experiment results show that when the target ridge height is 30 cm and 40 cm, the average standard deviation of ridge height is 0.98 cm and 0.97 cm respectively, and the qualified rate of ridge height is more than 94 %. It shows that the designed ridge height adaptive adjustment system can effectively track the height instruction, and significantly improve the ridge quality and operation stability under complex terrain.

摘要
针对丘陵山地地形起伏导致的起垄机适应性差及垄高稳定性不足的问题，本研究设计了一种履带式起垄机垄高自适应调节系统。通过分析起垄作业过程，建立垄高控制数学模型，采用基于增量式 PID 的控制策略实时动态调整液压缸推杆伸缩，实现了机具升降的精准调节。结合惯性测量单元实时采集车身俯仰角与高度信息，对起垄高度进行动态补偿。田间试验结果表明，在目标垄高为 30 cm 和 40 cm 时，垄高标准差平均值分别为 0.98 cm 和 0.97 cm，垄高合格率均超过 94%，表明所设计的垄高自适应调节系统能够有效跟踪高度指令，显著提高了复杂地形下的起垄质量与作业稳定性。

INTRODUCTION
Ridging and film mulching is critical for vegetable cultivation (*Hu et al., 2018; An et al., 2022; Yao et al., 2025*), enhancing soil aeration, light utilization, drought/waterlogging resistance, water/fertilizer retention, reducing pests/diseases, and boosting crop yield/quality. With precision agriculture development, higher requirements are placed on its operation quality and accuracy. In undulating fields, manual real-time ridge height adjustment increases labor intensity, necessitating automatic adjustment based on vehicle posture.

Most existing studies (*Tian et al., 2024; Zhang et al., 2014; Sui et al., 2016; Shi et al., 2022; Wang et al., 2020; Zhang et al., 2020*) focus on traditional ridger design/optimization, which fail to solve low ridging accuracy from ground undulations. In recent years, some researchers proposed an ExpressLRS-based autonomous navigation method to improve ridge straightness, but did not address flatness issues (Zhao, et al. *2025*). Meanwhile, researchers have developed a suspended machine with stepless ridge height adjustment (25–35 cm), but it lacks dynamic precision regulation for flatness issues caused by ground undulations (*Liu et al., 2023*).

Sensor technology offers solutions. Some researchers designed a spray boom leveling system using MEMS inertial sensors (*Zhang et al., 2019*). Additionally, some research teams have employed JY61P tilt sensors to achieve dynamic balance adjustment of spray booms through hydraulic cylinder actuation. Similar sensor-based attitude leveling technologies have now been extended to various types of agricultural machinery (*Yin et al.*, *2022*).

This study uses Hualong Technology's crawler-type ridger as the platform, developing an adaptive ridge height adjustment system. A low-cost, stable tilt sensor measures vehicle tilt angle. By fusing remote control, ridge height knob, and angle sensor signals, and applying incremental PID control and mechatronics technology, it controls hydraulic cylinder extension to maintain the ridging mechanism's absolute height, improving complex field adaptability and supporting unmanned driving/navigation.

MATERIALS AND METHODS

Ridge-building requirements

Significant climatic differences exist between northern and southern China, which directly influence the setting of ridge heights in crop cultivation. In the rainy southern regions, ridge heights are typically set at 25–40 cm to enhance field drainage and prevent waterlogging of crop roots. In contrast, in the arid northern regions, ridge heights can be appropriately reduced to 20–25 cm to balance soil moisture retention and tillage efficiency. Furthermore, ridge height varies with different types of vegetable cultivation: ridge heights for maize typically range from 10–30 cm; for kale, they generally fall between 25–30 cm; and for Zengcheng Late Heart Vegetable, the ridge height is usually around 30 cm (*Nie et al.*, *2022*). Consequently, ridgers must be equipped with ridge height adjustment functionality to meet the diverse agronomic requirements across different regions.

The topography in the hilly and mountainous areas of southern China is complex, with low land levelness (*Hao et al., 2022*), posing significant challenges to ridging operations. Traditional ridgers, lacking adaptive ridge height adjustment capabilities, are prone to significant variations in ridge smoothness due to ground undulations, making it difficult to ensure consistency in ridge height. As a key agricultural implement for pre-planting land preparation, a ridger must maintain uniform ridge height throughout the operation. Therefore, when working on fields with substantial topographic variation, the ridger needs to automatically adjust the ridge height to ensure uniformity and meet the agronomic needs for crop growth.

Principle of ridge height adaptive adjustment system for ridgers

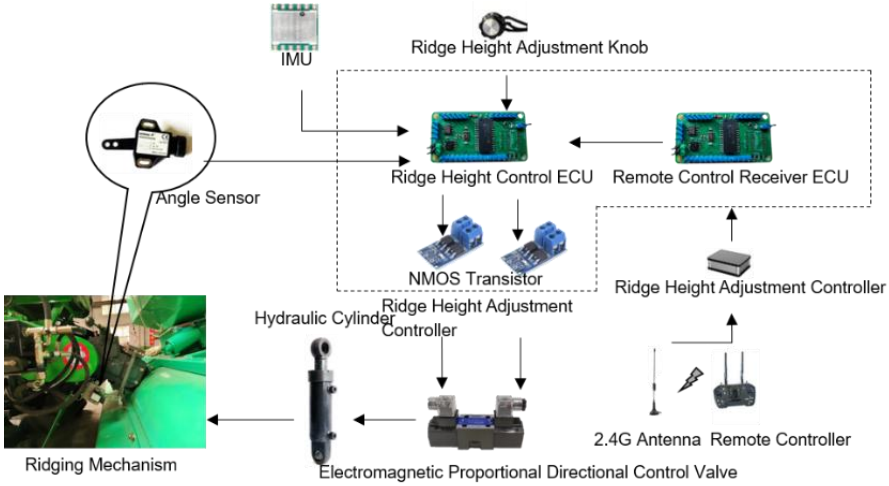

Fig. 1 - Ridge height adaptive control system

The ridge height adjustment system of the ridger is composed of a ridge height adjustment controller, an Inertial Measurement Unit (IMU) attitude sensor, a ridge height adjustment knob, an NMOS transistor, an electromagnetic proportional directional control valve, a hydraulic cylinder, an angle sensor, and a ridging mechanism. The controller supports two operating modes: manual mode and remote control mode. The system composition and working principle are shown in Figure 1.

In manual mode, the ridge height adjustment controller reads three signals in real time: the analog voltage value output by the ridge height adjustment knob, the vehicle body attitude signal output by the IMU, and the analog voltage value output by the angle sensor. After signal calculation, the controller controls the on-off state of the NMOS transistor to further regulate the opening and closing of the electromagnetic proportional directional control valve, realizing the telescopic movement of the hydraulic cylinder and thus completing the ridge height control.

In remote control mode, the remote control receiver accurately receives the ridge height adjustment command sent by the remote controller through a 2.4G antenna. After processing, the command is transmitted to the ridge height adjustment controller in a standardized data format via a TTL serial port. The controller compares this command with the output value of the IMU and the feedback value of the angle sensor, and then outputs a PWM signal to control the action of the NMOS transistor, thereby achieving ridge height adjustment.

Mathematical model of the ridge height adjustment mechanism

During the operation of the ridging and film mulching machine, the ridging mechanism must adjust the ridge height in real time to ensure uniform ridge height. To facilitate the analysis of its working principle, a mathematical model of the working mechanism is established, as shown in Figure 2. Point O_t is the hinge point between the rear side of the tractor and the implement, Point O_i is the hinge point between the hydraulic cylinder and the suspension mechanism, Point *C* is the position of the upper baffle of the ridging device, Point *B* is the projection of Point *C* on the ground, Point *D* is the hinge point between the hydraulic cylinder and the tractor body, and Point *A* is the intersection of the straight line O_t and the ground. For the convenience of analyzing the mathematical model, it is assumed that Points O_tD, and A lie on the same vertical line, and Points O_t, O_i, and *C* lie on a straight line.

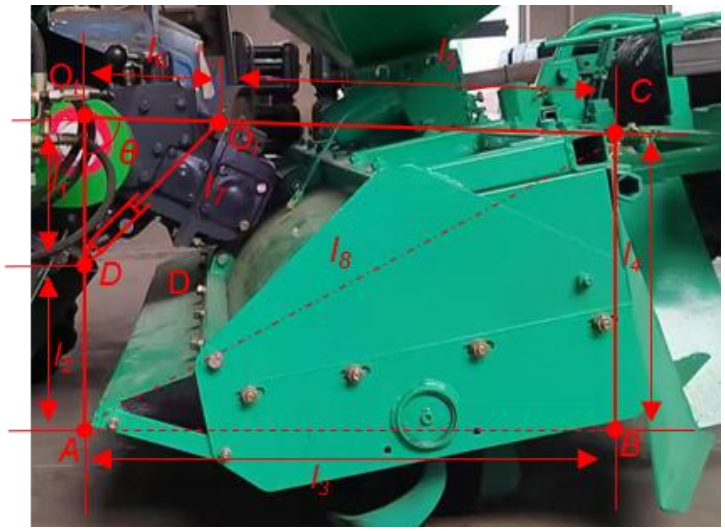

Fig. 2 - Mathematical model of ridge height adjustment actuator

The relationship between the angle θ between the suspension mechanism O_tC and O_tA and the hydraulic cylinder length l_7 is as follows:

$$\theta = \arccos \frac{l_6^{\,2} + l_1^{\,2} - l_7^{\,2}}{2 l_6 l_1} \tag{1}$$

Trigonometric functions yield the relationship between l_8 and θ:

$$\theta = \arccos \frac{(l_6 + l_5)^2 + (l_1 + l_2)^2 - l_8^{\,2}}{2(l_6 + l_5)(l_1 + l_2)} \tag{2}$$

$$l_8^{\,2} = l_3^{\,2} + l_4^{\,2} \tag{3}$$

$$l_4^{\,2} = (l_6 + l_5)^2 + (l_1 + l_2)^2 - 2(l_6 + l_5)(l_1 + l_2)\cos\theta - l_3^{\,2} \tag{4}$$

In the formula, θ denotes the included angle between O_tD and O_tC, l_1 is the length of O_tD, l_2 is the length of AD, l_3 is the length of AB, l_4 is the length of BC, l_5 is the length of O_iC, l_6 is the length of O_tO_i, l_7 is the length of O_iD, l_8 is the length of AC.

As shown in Figure 3, these are the limit positions where the hydraulic cylinder extends/retracts to its limit, i.e., the limit positions where the implement rotates counterclockwise/clockwise around O_t.

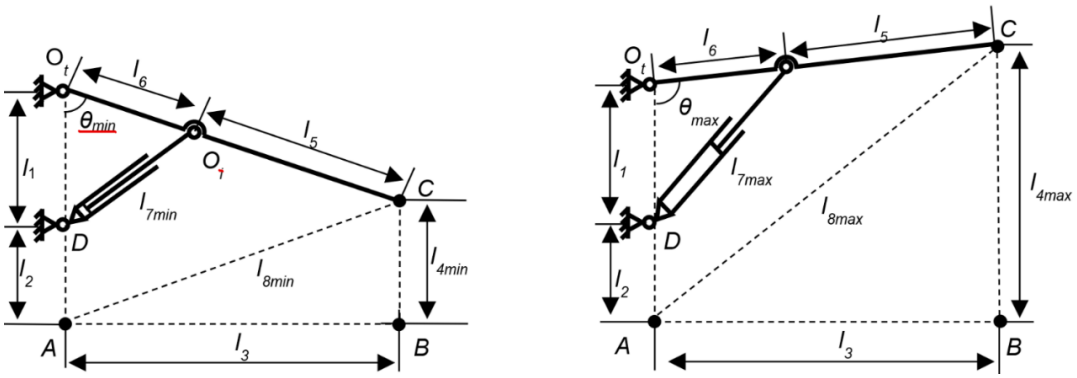

Fig. 3 - Extreme positions of hydraulic cylinder extension and retraction

(a) Limit Retracted Position of Hydraulic Cylinder; (b) Limit Extended Position of Hydraulic Cylinder

Assuming the maximum length of the hydraulic cylinder is $l_{7\max}$ and its minimum length is $l_{7\min}$, the following can be derived:

$$\begin{cases} \theta_{\max} == \arccos \dfrac{l_6^{\,2} + l_1^{\,2} - l_{7\max}^{\,2}}{2 l_6 l_1} \\ \theta_{\min} == \arccos \dfrac{l_6^{\,2} + l_1^{\,2} - l_{7\min}^{\,2}}{2 l_6 l_1} \\ \Delta\theta = \theta_{\max} - \theta_{\min} \end{cases} \tag{5}$$

The adjustment range of the ridge height is as follows:

$$\begin{cases} l_{4\max} = \sqrt{(l_6 + l_5)^2 + (l_1 + l_2)^2 - 2(l_6 + l_5)(l_1 + l_2)\cos\theta_{\max} - l_3^{\,2}} \\ l_{4\min} = \sqrt{(l_6 + l_5)^2 + (l_1 + l_2)^2 - 2(l_6 + l_5)(l_1 + l_2)\cos\theta_{\min} - l_3^{\,2}} \\ \Delta l = l_{4\max} - l_{4\min} \end{cases} \tag{6}$$

Among them, $\theta_{\max}$, $\theta_{\min}$ and $\Delta\theta$ represent the maximum angle, minimum angle, and angular adjustment range of θ respectively; $l_{4\max}$, $l_{4\min}$ and Δl_4 denote the maximum height, minimum height, and ridge height adjustment range of l_4 respectively.

Implement's automatic leveling controller design

Hardware design

Based on the ridge height adjustment system's working principle, the adaptive ridge height adjustment controller needs to determine the operating mode, read analog voltages from the remote control handle, ridge height adjustment knob and angle sensor, acquire vehicle body attitude information, and output PWM signals to drive NMOS transistors on/off. Accordingly, the controller shown in Figure 4 is designed.

The adaptive ridge height adaptive adjustment controller is centered on the PIC18F258 processor, with its CAN bus physical interface provided by the PCA82C250 chip. The IMU is a JY61P inertial measurement unit, featuring an output frequency of 20 Hz and supporting UART serial output mode. The signal output port D1 of the ridge height adjustment knob is connected to the analog input interface A0 of the processor. The output port D2 of the angle sensor is connected to the analog input interface A1 of the processor. The processor controls the on-off status of two NMOS transistors via I/O ports C0/C1. The input voltage of the NMOS transistors is 12 V, and their output ends are connected to the electromagnetic proportional directional control valve. When the control end of an NMOS transistor receives a low-level signal, its input and output ends are turned on; when it receives a high-level signal, its input and output ends are turned off. The voltage conversion module converts 12 V DC power into 5 V DC power required by the control system. K1 is the main power switch. K2 is the working state switch for switching between manual and remote-control modes: when K2 is disconnected, the input at pin B1 is high-level, corresponding to manual mode; when K2 is closed, the input at pin B1 is low-level, corresponding to remote control mode.

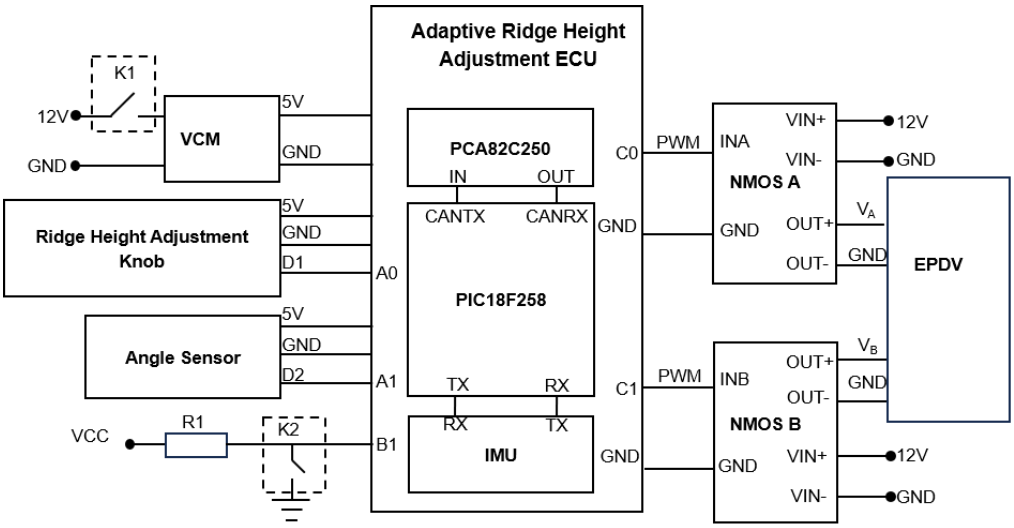

Fig. 4 - Principle of Ridge Height Adaptive Adjustment Controller

VCM is Voltage Conversion Module; EPDV is Electromagnetic Proportional Directional Valve

Software design

The automatic control program for the ridge height adjustment system was developed in C. After system startup, the main program runs at fixed intervals. It performs the calibration of the target ridge height, calculates the current ridging angle from the analog voltage output of the angle sensor, and computes the current ridge height based on this angle. Following filtering, the program drives the NMOS transistor to operate. The coordinated interaction of the solenoid directional valve and hydraulic cylinder modules enables closed-loop control of the ridge height. The specific control flowchart is shown in Figure 5.

After system startup, an initialization routine is executed to calibrate the vehicle body attitude, which is then set as the initial reference frame. The system subsequently identifies its operational mode and configures the target ridge height l_a and the angle adjustment threshold n.

The Inertial Measurement Unit (IMU) then acquires real-time data, measuring the current body inclination angle β_α and altitude h_α, concurrently detecting the instantaneous ridging angle θ_α.

Using the inputs of current body inclination θ_α, IMU-measured height h_α, and the preset target height l_a, the system calculates the desired ridge height l_β. This value is then converted into a corresponding desired ridging angle θ_β.

A closed-loop control logic is implemented: the absolute error between the current ridging angle θ_α and the desired angle θ_β is computed. If this error exceeds the permissible threshold n, the controller generates a high/low logic signal. This signal drives an NMOS transistor switch to actuate a solenoid valve, thereby controlling the extension or retraction of a hydraulic cylinder. The adjustment continues iteratively until the absolute error is minimized to within the specified threshold n.

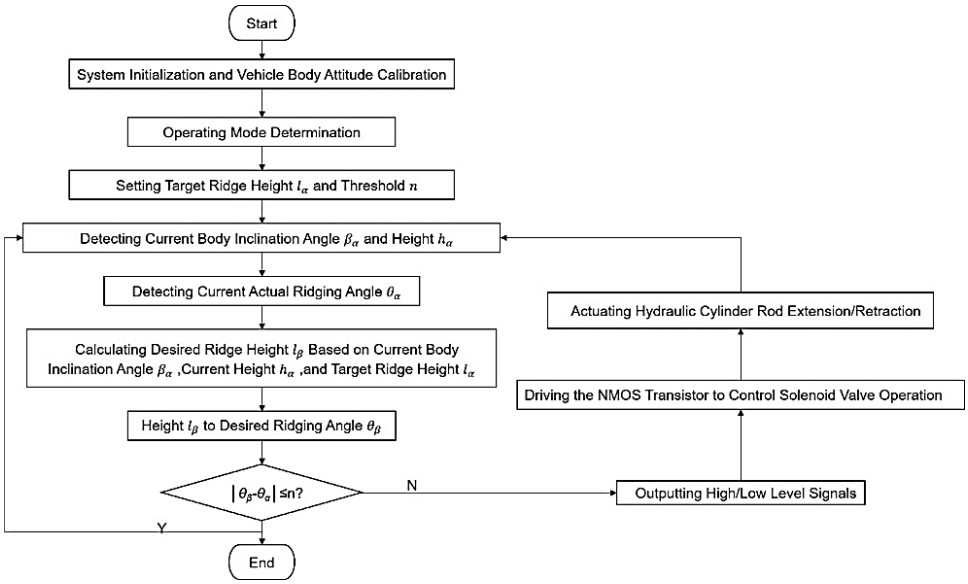

Fig. 5 - System control flow chart

Ridge height compensation and control method

During field operations, due to the complex terrain environment, it is necessary to measure the vehicle body attitude to compensate for the ridge height. In this study, the vehicle body height and pitch information are obtained through the IMU, and compensation is performed to achieve a stable height effect. For the convenience of analysis, the entire vehicle is simplified into the mathematical model shown in Figure 6, which is observed from the left side of the vehicle body. Among them, Point D is the installation position of the IMU.

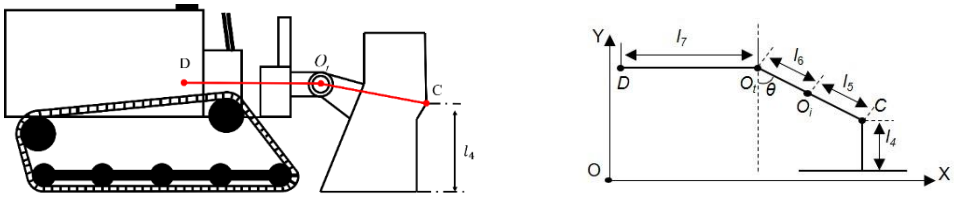

Fig. 6 - Simplification of the Vehicle Model

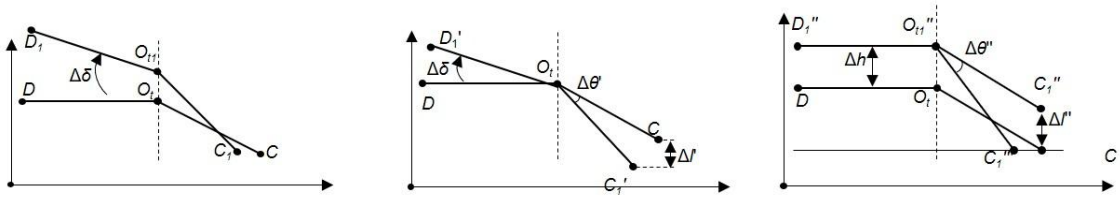

Fig. 7 - Decomposition of Vehicle Body Disturbance

a) Total Vehicle Body Disturbance; b) Vehicle Body Pitching Motion; c) Displacement Along the Y-Direction

When the ridger is disturbed by the road surface, the height information and angle information collected by the IMU will change as shown in Figure 7(a). The attitude information can be converted into the pitching motion of the vehicle body along the Y-axis, as illustrated in Figure 7(b), and the displacement motion of the vehicle body, as shown in Figure 7(c).

When the vehicle body rotates clockwise by $\Delta\delta$ due to ground disturbance (i.e., DO_t rotates to $D_1'O_t$), O_tC simultaneously rotates to O_tC_1' , as shown in Figure 7(b). To keep the ridge height constant, it is necessary to extend the hydraulic cylinder to rotate the suspension mechanism counterclockwise by $\Delta\theta'$, whose value is:

$$\Delta\theta' = \Delta\delta \tag{7}$$

When the vehicle body displaces by Δh along the Y-direction, as shown in Figure 7(c), the ridge height changes by $\Delta l''$ simultaneously, and its value is:

$$\Delta l'' = \Delta h \tag{8}$$

To offset the impact caused by the vehicle body's displacement along the Y-axis, C_1'' needs to rotate by $\Delta\theta$'' around point O_{t1}'' to C_1'''. With clockwise θ defined as positive and counterclockwise as negative, the value of $\Delta\theta$'' is:

$$\Delta\theta'' = \theta_a - \arccos(\cos\theta_a - \frac{\Delta l'' - (h_{d1} - l_7\sin\Delta\delta)}{l_5 + l_6}) \tag{9}$$

At the next moment, the corrected theoretical angle shall be:

$$\theta_t = \theta_b - \Delta\theta'' + \Delta\theta' \tag{10}$$

where: θ_a is the angle value measured by the angle sensor; θ_b is the angle value sent by the ridge height adjustment knob or remote controller; θ_t is the corrected theoretical angle value; h_{d1} is the IMU height; l_7 is the length of D_1O_{t1}.

For stable ridge height control, an incremental PID algorithm (*Xu et al., 2022; He et al., 2021; Huang et al., 2025; Cao et al., 2025; Liu et al., 2023; Wang et al., 2024)* is used. It takes the difference e between the corrected theoretical angle and the angle sensor's measurement as input, calculates the control signal u, and sends it as PWM signals to NMOS transistors. By controlling their on/off, it drives the electromagnetic proportional directional valve to actuate hydraulic cylinder extension/retraction, offsetting the ridge angle

difference. The controller compares the corrected theoretical angle θ_t with the sensor-measured angle θa, calculates the angle difference e_i via Formula (11), and controls the two NMOS transistors: NMOS A turns on when $e_i > 0$, NMOS B when $e_i < 0$ (both reducing e_i to near zero); both turn off when $e_i = 0$.

$$e_i = \theta_t - \theta_{ai} \tag{11}$$

$$u(i) = K_p \cdot e(i) + K_i \cdot \left[e(i) - 2e(i-1) + e(i-2)\right] + K_d \cdot \left[e(i) - e(i-1)\right] \tag{12}$$

where: θ_{ai} is the actual ridge-forming angle at the i-th sampling K_p, K_i, K_d are the proportional, integral, and derivative coefficients of PID control respectively: e_i, e_{i-1}, e_{i-2} are the angle differences at the i-th, (i-1)-th, and (i-2)-th samplings respectively; $u(i)$ is the control signal output by the incremental PID algorithm.

Experimental Methods

To verify the system's control accuracy, the ridge top flatness was measured in accordance with the ridge operation quality measurement method specified in Technical Specifications for Mechanized Ridge Operation in Vegetable Tillage and Land Preparation, using a straightedge to measure the vertical height difference of different measuring points on the ridge top relative to the reference plane. Three groups of tests were conducted for ridge heights of 30 cm and 40 cm respectively, with each group operating three 10-meter-long ridges (a, b, c) as shown in Figure 8.(b) 100 measuring points were taken at 10 cm intervals on each ridge, and each point was measured three times to take the average value for data recording.

RESULTS

Test Scenario

To evaluate the control accuracy and stability of the designed adaptive ridge height adjustment device, a field test was conducted in Hualong Test Field, Qingzhou City, Weifang City, Shandong Province in July 2025. The test was carried out on the self-propelled ridger independently developed by Hualong Agricultural Equipment Co., Ltd., as shown in Figure 8 (a) The adaptive ridge height adjustment system was installed on the test platform and initially debugged. The adaptive ridge height adjustment controller, together with the vehicle controller, was encapsulated in the overall machine controller. The test results are shown in Figure 8 (b).

To verify the system's control accuracy, the ridge top flatness was measured in accordance with the ridge operation quality measurement method specified in Technical Specifications for Mechanized Ridge Operation in Vegetable Tillage and Land Preparation, using a straightedge to measure the vertical height difference of different measuring points on the ridge top relative to the reference plane. Three groups of tests were conducted for ridge heights of 30 cm and 40 cm respectively, with each group operating three 10-meter-long ridges (a, b, c) as shown in Figure 8(b) 100 measuring points were taken at 10 cm intervals on each ridge, and each point was measured three times to take the average value for data recording.

a) Experimental Platform b) Test Results

Fig. 8 - Experimental Platform and Test Results

1.Positioning and Directional Antenna; 2. Operation Terminal; 3. Agricultural Machinery Whole-Machine Controller

Field Test Results

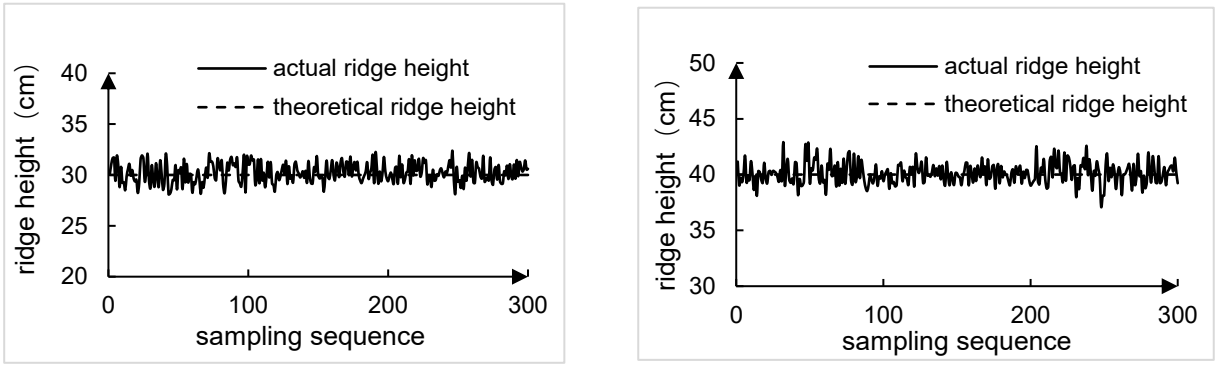

a) Measured Results of Target Ridge Height (30 cm) b) Measured Results of Target Ridge Height (40 cm)

Fig. 9 - Field experiment results

Field test results are shown in Figure 9 (sampling sequences 0-100 for Ridge a, 101-200 for Ridge b, 201-300 for Ridge c), with their average values, ridge height qualification rates and standard deviations summarized in Table 1. According to the agronomic requirements for mechanized planting of solanaceous crops, the criteria for qualification are: ridge height error within ±2 cm with a qualification rate ≥80%, and ridge top flatness (expressed by standard deviation) <2.5 cm. Table 1 indicates that at 30 cm ridge height, the qualification rates are 98%, 99% and 98%, and the flatness values are 1.14 cm, 0.89 cm and 0.89 cm; at 40 cm ridge height, the qualification rates are 94%, 100% and 94%, and the flatness values are 1.05 cm, 0.71 cm and 1.10 cm. For both target ridge heights, the average standard deviations are 0.98 cm and 0.97 cm respectively, with qualification rates all exceeding 94%. This demonstrates that the designed adaptive ridge height adjustment system can effectively track height commands, significantly improving ridge quality and operational stability under complex terrain.

Table 1

Experimental results of ridge height

Ridge Height	Ridge Number	Average Value	Ridge Height Qualification Rate	Standard Deviation
		cm	%	cm
30 cm	1	30.12	98	1.14
	2	30.27	99	0.89
	3	30.25	98	0.89
40 cm	1	40.09	94	1.05
	2	40.06	100	0.71
	3	40.15	94	1.10

The slight performance divergence between the 30 cm and 40 cm ridge height configurations stems from two primary causes. First, mechanical load properties of the ridger are dependent on ridge height. For 40 cm ridge formation, the greater soil volume requiring lifting and shaping optimizes the stress distribution of the machine's soil-contacting components, ensuring more stable operation. Conversely, the smaller soil handling volume in 30 cm ridge construction induces more pronounced load fluctuations on the working parts, which marginally impairs ridge height control consistency and thus reduces flatness performance to a small extent. Second, the adaptive PID control system exhibits differential response sensitivities to height deviations of varying scales. The 40 cm target height corresponds to a wider absolute height adjustment range, allowing the incremental PID controller to deliver more refined regulation of the system's dynamic response during large-stroke adjustments. In contrast, the narrower adjustment range for 30 cm ridges makes the controller more susceptible to minor overshoots due to its heightened sensitivity to small deviations, resulting in a slight uptick in the flatness standard deviation. Notably, these discrepancies fall within an acceptable range, and both ridge height settings fully meet agronomic operational requirements, which attests to the robust adaptability of the developed system.

CONCLUSIONS

To address the issue that existing self-propelled ridgers are prone to poor ridging flatness due to terrain influences when operating in complex, highly undulating fields, an adaptive ridge height adjustment system with both manual and automatic control functions was designed, which can automatically adjust ridge height according to terrain undulations.

(1) Based on the requirements for ridge height in solanaceous crop planting and the structural principles of the operating mechanism, a ridge height adjustment control device was designed to control ridge height by regulating the extension and retraction of the hydraulic cylinder.

(2) A ridge height control algorithm based on incremental PID was developed to enable the actual ridge height to quickly reach the target height, and it can adjust the ridging height in real time according to the vehicle body attitude information detected by the IMU.

(3) Test results indicate that the qualification rates meet the specified standards when the ridge height is set to 30 cm and 40 cm: both exceed 80%, with the ridge top flatness significantly below the 2.5 cm standard. Thus, the ridging and film mulching machine equipped with the adaptive ridge height adjustment system can meet the ridging demands in complex field environments, providing technical support for the unmanned driving and automatic navigation of ridgers.

REFERENCES

[1] An, H., Liu, W., Yu, Z., Qin H., Shen S., Hu H., Zhang JK., Jin C. (2022). Comparative analysis of operation performance of different types of lettuce ridgers (不同形式生菜起垄机作业对比分析). *Agricultural Machinery Technology Extension*, (12), 42-45.

[2] Cao, X., Zheng, Y., Xiao, H., Xiao, M., (2025). Multi-Target Point Path Planning and Tracking of Unmanned Surface Vehicle Using SFLOS Algorithm and Incremental PID Control with Crane-Assisted. *IEEE Access*, *13*, 44620–44635. https://doi.org/10.1109/ACCESS.2025.3549377

[3] Du, H., Luo, X., (2025). Design of a Full Static Pressure Control System Based on Incremental PID (基于增量式 PID 的全静压控制系统设计). *Modern Electronics Technique*, 48(12), 6-12.

[4] Hao, D., Li, J., Yu, M., (2022). Analysis on the Influence of Different Ridge Heights on the Growth and Development of Flue-cured Tobacco under Deep Tillage Conditions (深耕条件下地烟不同垄高对烤烟生长发育影响分析). *Seed Science and Technology*, 40(14), 27-29.

[5] Huang, Y., Lin, Y. (2025). A MCU based four-switch buck-boost converter with incremental PID control. *IET Conference Proceedings*, 2025(15), 9–12. https://doi.org/10.1049/icp.2025.2473

[6] Hu, J., Zhang, W., Yan, W., Ji Y., Hu MJ., Li K. (2018). Research status and prospect of sweet potato ridging machinery at home and abroad (国内外甘薯起垄机械研究现状与展望). *Journal of Chinese Agricultural Mechanization*, 39(11), 12-16.

[7] Liu, D., Hu, J., Gong, Y., Chen X., Wang G., Zhang X. (2023). Design and experiment of suspended rotary tillage ridge and film mulching machine, *INMATEH - Agricultural Engineering* 69(1), pp. 237-244, https://doi.org/10.35633/inmateh-69-22

[8] Nie, H., Zhang, J., (2024). Exploration and Optimization of Mechanization Technology for Key Links of Vegetable Cultivation in Southern Hilly and Mountainous Areas (南方丘陵山区蔬菜关键环节机械化技术的探索与优化). *Agricultural Machinery Technology Extension*, (10), 28-30.

[9] Shi Y., Chen, X., Chen, M., Wang D.W., Shang S.Q. (2022). Design and Experiment of Plowshare-type Ditching and Ridging Device for Sweet Potato Ridging and Shaping Machine(甘薯起垄整形机犁铧式开沟起垄装置设计与试验). *Transactions of the Chinese Society for Agricultural Machinery*, 53(10), 16-25.

[10] Sui X., (2016). Design and Experimental Study on Sweet Potato Ridging and Film Mulching Machine (甘薯起垄覆膜机的设计与试验研究). Qingdao Agricultural University, Qingdao, China.

[11] Tian, J., Lin, Y., Liu, Y., Yang FH., Xu S.H., Luo H.H., Miao Q.Y., Zeng S. (2024). Development of an Integrated Machine for Ridging, Fertilizing and Film Covering(起垄施肥覆膜一体机的研制). *Modern Agricultural Equipment*, 45(06), 22-27+41.

[12] Wang, W., He, G., Wang, Y., Wang Y.N., Wang P., Luo P.S. (2020). Design and Experimental Study on Chili Ridging and Film Mulching Machine(辣椒起垄覆膜机的设计与试验研究). *Journal of Agricultural Mechanization Research*, 42(6), 57-62.

[13] Wang, Z., Zhang, J., (2024). Incremental PID Controller-Based Learning Rate Scheduler for Stochastic Gradient Descent. *IEEE Transactions on Neural Networks and Learning Systems*, *35*(5), 7060–7071. https://doi.org/10.1109/TNNLS.2022.3213677

[14] Xu Y., Zhou K., Yang Y., Yang Q., Xiang JY. (2022). Design of Stepper Motor Speed Control System Based on Incremental PID (基于增量式 PID 的步进电机速度控制系统设计). *Science and Technology & Innovation*, (01), 172-175+178.

[15] Yao D.W., Lu Y., Wang Y.F., Lu Z.X. (2025). Design and experiment of ridge planting tuber harvester(起垄种植茎块收获机的设计与试验). *Journal of Agricultural Mechanization Research*, 47(08), 112-118+139.

[16] Yin X., An J.H., Wang X., Wang Y.L., Li J.Q., Jin CQ (2022). Design and experiment of automatic leveling system for spray boom of high-clearance sprayer(高地隙施药机喷杆自动调平系统设计与试验). *Transactions of the Chinese Society for Agricultural Machinery*, 53(02), 98-105+115.

[17] Zhang A., Li X., (2014). Experimental Study on Ridge-Film Mulching Cultivation of Maize(玉米起垄覆膜栽培试验研究). *Modern Rural Science and Technology*, (04), 64-65.

[18] Zhang M., Hu L., Ke X., Ke X.R., Tang LM., Meng SB., Du P., Zhou H., He J. (2019). Design and experiment of automatic leveling system for spray boom of self-propelled paddy field sprayer(水田自走式喷雾机喷杆自动调平系统设计与试验). *Journal of Agricultural Mechanization Research*, 41(10), 45-51.

[19] Zhang S.L., Zhao W.Y., Dai F., Song X.F., Zhai J.F., Zhang F.W. (2020). Simulation Analysis and Experiment on Pressing Operation Process of Full-film Double Ridge Furrow Ridging and Film Mulching Machine(全膜双垄沟起垄覆膜机镇压作业过程仿真分析与试验). *Transactions of the Chinese Society of Agricultural Engineering*, 36(1), 20-30.

[20] Zhao K.X., Tian SB., Ning X.F., Tao L. (2025). Design and Experiment of Autonomous Navigation Ridging and Film Mulching Machine Based on ExpressLRS (基于 ExpressLRS 的自主导航起垄覆膜机设计与试验). *Transactions of the Chinese Society for Agricultural Machinery*, 56(06), 330-340.